remote sensing

MDPI

Article

Real-Time Tropospheric Delays Retrieved from Multi-GNSS Observations and IGS Real-Time Product Streams

Cuixian Lu [1,2,*], Xinghan Chen [1], Gen Liu [2], Galina Dick [1], Jens Wickert [1], Xinyuan Jiang [1], Kai Zheng [1,2] and Harald Schuh [1]

1 Division of GPS/Galileo Earth Observation, German Research Centre for Geosciences (GFZ), Telegrafenberg, 14473 Potsdam, Germany; xchen@gfz-potsdam.de (X.C.); dick@gfz-potsdam.de (G.D.); wickert@gfz-potsdam.de (J.W.);jxinyuan@gfz-potsdam.de (X.J.); zhengkai@whu.edu.cn (K.Z.); schuh@gfz-potsdam.de (H.S.)

2 Department of Surveying Engineering, Wuhan University, 129 Luoyu Road, Wuhan 430079, China; gliu@whu.edu.cn

* Correspondence: cuixian@gfz-potsdam.de; Tel.: +49-331-288-1113

Received: 20 October 2017; Accepted: 13 December 2017; Published: 15 December 2017

Abstract: The multi-constellation Global Navigation Satellite Systems (GNSS) offers promising potential for the retrieval of real-time (RT) atmospheric parameters to support time-critical meteorological applications, such as nowcasting or regional short-term forecasts. In this study, we processed GNSS data from the globally distributed Multi-GNSS Experiment (MGEX) network of about 30 ground stations by using the precise point positioning (PPP) technique for retrieving RT multi-GNSS tropospheric delays. RT satellite orbit and clock product streams from the International GNSS Service (IGS) were used. Meanwhile, we assessed the quality of clock and orbit products provided by different IGS RT services, called CLK01, CLK81, CLK92, GFZC2, and GFZD2, respectively. Using the RT orbit and clock products, the performances of the RT zenith total delays (ZTD) retrieved from single-system as well as from multi-GNSS combined observations were evaluated by comparing with the U.S. Naval Observatory (USNO) final troposphere products. With the addition of multi-GNSS observations, RT ZTD estimates with higher accuracy and enhanced reliability compared to the single-system solution can be obtained. Compared with the Global Positioning System (GPS)-only solution, the improvements in the initialization time of ZTD estimates are about 5.8% and 8.1% with the dual-system and the four-system combinations, respectively. The RT ZTD estimates retrieved with the GFZC2 products outperform those derived from the other IGS-RT products. In the GFZC2 solution, the accuracy of about 5.05 mm for the RT estimated ZTD can be achieved with fixing station coordinates. The results also confirm that the accuracy improvement (about 22.2%) can be achieved for the real-time estimated ZTDs by using multi-GNSS observables, compared to the GPS-only solution. In the multi-GNSS solution, the accuracy of real-time retrieved ZTDs can be improved by a factor of up to 2.7 in the fixing coordinate mode, compared with that in the kinematic mode.

Keywords: multi-GNSS; tropospheric delays; IGS-RT; orbit and clock products; precise point positioning

1. Introduction

Water vapor, as a fundamental component of the atmosphere, plays a key role in the hydrological cycle and the climate system. Traditional water vapor measurements are mainly provided by the meteorological sensors, such as radiosondes and water vapor radiometers [1,2]. However, due to the high spatiotemporal variability of the atmospheric water vapor and limitations of these traditional observing techniques, efforts have been made to obtain reliable and enhanced water vapor observations.

Global Positioning System (GPS) meteorology conceived as monitoring the atmospheric water vapor with ground-based GPS receivers was firstly introduced in 1990s [3]. Since then, extensive studies concerning GPS meteorology have been carried out in the past two decades. The results demonstrated the capability of GPS for providing water vapor estimates with comparable accuracy to those offered by the meteorological sensors [4–6]. Furthermore, the GPS-derived water vapor also has its advantages, such as low operational expense, high spatiotemporal resolution, and all-weather availability.

Most of these previous investigations were limited to post-processing and near-RT modes, while few studies involve the RT mode, which requires an efficient RT service system that offers RT orbits, satellite clocks, and other RT products [7]. However, with the increasing innovative applications, nowcasting and short-term weather forecasting have been becoming important trends in meteorology this requires more information of the atmosphere state being provided with short or even no latency [7,8]. To deliver the tropospheric products in RT serving for the time-critical operational meteorology has become one of the focuses within the GNSS (Global Navigation Satellite Systems) meteorology community. Attributing to the recent development of the IGS (International GNSS Service) RT pilot project (RTPP), the RT satellite orbit/clock products provided by IGS, as well as its analysis centers (ACs) such as GeoForschungsZentrum (GFZ) and the European Space Agency (ESA), are now available for scientific researches and projects. This offers a good potential for estimating the tropospheric delays by using the RT PPP [9–12].

Dependent on the IGS-combined RT satellite orbit/clock products, the European Coordination in Science and Technology (COST) has started to offer the RT zenith total delay (ZTD) products on the basis of GPS observations. Meanwhile, the RT Demonstration campaign (RT-Demo) is organized by Working Group 1 "Advanced GNSS Tropospheric Products" of the COST ES1206 Action GNSS4SWEC ("Advanced Global Navigation Satellite Systems tropospheric products for monitoring severe weather events and climate") [13]. This campaign was designed in 2014 and officially began on 1 April 2015, and aims at fully exploiting the current GNSS capability for the RT meteorological applications. Some of the recent studies have concentrated on retrieving the RT tropospheric products or water vapor based on GPS-only observations. The results pointed out that the high accuracy (a few millimeters) of the derived RT tropospheric delays or water vapor can be achieved when compared to the post-processing products and meteorological data [7,11,12].

Nowadays, the world of the satellite navigation system is undergoing rapid development into a powerful multi-GNSS constellation, along with the modernization of GPS, the recovery of the Russian Global Navigation Satellite System (GLONASS), and the newly developing European Galileo and the Chinese Beidou satellite (BDS) system [13]. As of September 2017, more than 90 navigation satellites (32 GPS, 24 GLONASS, 18 BDS, 18 Galileo) are in orbit and transmitting data profiting from the multi-GNSS constellation. Moreover, the number of the satellites in total will increase to more than 120 once all four systems (GPS, GLONASS, Galileo, and BDS) are fully deployed. Many of the GPS networks have been upgraded to the multi-GNSS observation networks. As an example, the IGS MGEX network, consisting of more than 120 stations, was deployed in 2012 to facilitate the experiment with the emerging multi-system and multi-frequency data and to provide a well-established multi-GNSS service [14].

When compared with the single-system constellation, RT tropospheric products with enhanced availability, stability, and accuracy are anticipated from the fusion of multi-GNSS due to the increased number and the improved spatial geometry of the tracked satellites. The performance of RT tropospheric delays derived from multi-GNSS processing in the simulated RT mode has been investigated in some recent studies [8,15]. For example, Lu et al. performed a GPS + BDS combined solution for the RT water vapor retrieval and demonstrated that the accuracy of the derived water vapor could be improved from 1.7–2.1 mm to 1.5–1.8 mm when applying the combined instead of the GPS-only solution [8]. The RT water vapor retrieved from the four-system multi-GNSS combination (GPS + GLONASS + Galileo + BDS) was also studied by Li et al. [15]. The results showed that the water vapor estimates with higher accuracy (1.0–1.5 mm) and stronger reliability could be achieved from the

multi-GNSS fusion when compared to the single-system solutions (e.g., GPS-only, GLONASS-only, and BDS-only).

The latest investigation on multi-GNSS tropospheric delays retrieval in operational RT mode was carried out by Ding et al. [16]. They extracted RT ZTD estimates based on GPS, GLONASS, and Galileo observations employing the Precise Point Positioning (PPP) technology. In their study, the Precise Point Positioning with Integer and Zero-difference Ambiguity Resolution Demonstrator (PPP-WIZARD) software offered by the Centre National d'Etudes Spatiales (CNES) [17] was utilized, and the applied RT satellite orbit/clock products also were provided by from CNES.

In this contribution, GPS, GLONASS, Galileo, and BDS observations are incorporated together for the operational RT tropospheric monitoring based on the PPP approach. The RT iPPP software [10] is employed for data processing, and the satellites orbit/clock products provided by different IGS-RT analysis centers (e.g., BKG, GFZ) are utilized. Firstly, an experiment over 15 days is conducted to evaluate the performance of the RT satellites orbit/clock products from each IGS-RT service. The convergence time and the accuracy of RT ZTD estimates are assessed when applying different IGS-RT products. Then, the performance of RT ZTD retrieved from both single systems and from different multi-GNSS combination (concerning the weighting scheme for multi-system fusion, especially the contribution of BDS and Galileo) are investigated. Finally, the validation and comparison of different GNSS RT ZTD is carried out by using the IGS post-processing tropospheric products with high accuracy as reference.

2. Multi-GNSS ZTD Estimation in Real-Time

In the RT multi-GNSS PPP processing, the linearized equations of undifferenced (UD) carrier phase and pseudo-range observations can be expressed as follows,

$$\begin{cases} P^G_{r,j} = -\mathbf{u}^G_r \cdot x + t_r - {}^G - t^G + \kappa_{jG} \cdot I^G_{r,1} + T^G_r + c \cdot d_{rG} + e^G_{r,j} \\ P^{R_k}_{r,j} = -\mathbf{u}^R_r \cdot x + t_r - {}^R - t^R + \kappa_{jR_k} \cdot I^R_{r,1} + T^R_r + c \cdot d_{rR_k} + e^R_{r,j} \\ P^E_{r,j} = -\mathbf{u}^E_r \cdot x + t_r - {}^E - t^E + \kappa_{jE} \cdot I^E_{r,1} + T^E_r + c \cdot d_{rE} + e^E_{r,j} \\ P^C_{r,j} = -\mathbf{u}^C_r \cdot x + t_r - {}^C - t^C + \kappa_{jC} \cdot I^C_{r,1} + T^C_r + c \cdot d_{rC} + e^C_{r,j} \end{cases} \tag{1}$$

$$\begin{cases} L^G_{r,j} = -\mathbf{u}^G_r \cdot x + t_r - {}^G - t^G - \kappa_{jG} \cdot I^G_{r,1} + T^G_r + \lambda_{jG}(N^G_{r,j} + b_{rG,j} - b_j{}^G) + \varepsilon^G_{r,j} \\ L^{R_k}_{r,j} = -\mathbf{u}^R_r \cdot x + t_r - {}^R - t^R - \kappa_{jR_k} \cdot I^R_{r,1} + T^R_r + \lambda_{jR_k}(N^R_{r,j} + b_{rR_k,j} - b_j{}^R) + \varepsilon^R_{r,j} \\ L^E_{r,j} = -\mathbf{u}^E_r \cdot x + t_r - {}^E - t^E - \kappa_{jE} \cdot I^E_{r,1} + T^E_r + \lambda_{jE}(N^E_{r,j} + b_{rE,j} - b_j{}^E) + \varepsilon^E_{r,j} \\ L^C_{r,j} = -\mathbf{u}^C_r \cdot x + t_r - {}^C - t^C - \kappa_{jC} \cdot I^C_{r,1} + T^C_r + \lambda_{jC}(N^C_{r,j} + b_{rC,j} - b_j{}^C) + \varepsilon^C_{r,j} \end{cases} \tag{2}$$

where the indices G, R, E and C refer to the GPS, GLONASS, Galileo, and BDS satellites, respectively; R_k expresses the GLONASS satellite with frequency factor k; s, r, and j represent satellite, receiver, and frequency, respectively; P and L denote "observed minus computed" pseudorange and phase observables, respectively; $\mathbf{u}^s_r$ is the unit vector of the direction from receiver to satellite; x is the positioning error of station coordinates; ^{s} and t^s refer to the RT satellite orbit errors and satellite clock errors, respectively; t_r denotes the clock errors of receiver; $d_{r,s}$ is the code biases; $N^s_{r,j}$ is the integer ambiguity; $b_{r,j}$ and $b_j{}^s$ are the uncalibrated phase delays; λ_{js} is the wavelength; the ionospheric delays $I^s_{r,j}$ at different frequencies can be expressed as $I^s_{r,j} = \kappa_j \cdot I^s_{r,1} (\kappa_j = \lambda_j{}^2/\lambda_1{}^2)$; T^s_r represents the slant tropospheric delay; $e^s_{r,j}$ and $\varepsilon^s_{r,j}$ represent the sum of measurement noise and multipath error for the pseudorange and carrier phase observations. The phase center offsets and variations, tidal loading and phase wind-up are also considered using the existing models with sufficient accuracy [18]. For the phase center offset (PCO) and phase center variation (PCV) correction of receivers' antennas, the GPS values are used.

Because of the different frequencies and signal structure of the individual GNSS, the code biases for the four systems are different from each other in one multi-GNSS receiver. Thus, both inter-system bias (ISB) and inter-frequency bias (IFB) must be taken into account in a combined processing of

multi-GNSS observations. The code bias for GPS satellites is set to zero in order to eliminate the singularity between receiver clock and code bias parameters. In other words, all the estimated code biases for the other systems are relative to the biases of the GPS satellites.

For the RT multi-GNSS PPP processing, precise satellite orbits and clocks have to be firstly determined using the observation data from a global GNSS ground tracking network. Similar to the procedure of the IGS ultra-rapid orbits, the RT orbits are predicted (here 6-h prediction) based on the orbits determined in a batch-processing mode by using an orbit integrator. Afterwards, RT satellite clocks are estimated with fixed satellite orbits and station coordinates and updated epoch by epoch due to their short-term fluctuations [19]. The zero mean conditions over the ISB/IFB parameters are also introduced for each system (i.e., BDS and Galileo) and for each GLONASS frequency in the multi-GNSS orbit and clock determination [20]. In the combined data processing, suitable weighting of phase and pseudorange observables among systems should be considered carefully based on their qualities. An elevation-dependent weighting strategy is applied for the combined data processing of four-system observations. The stochastic model of UD pseudorange and carrier phase observations can be described as Equation (3):

$$\begin{gathered} Cov(i,j) = \begin{cases} \sigma_s^2 & (i=j) \\ 0 & (i \neq j) \end{cases} \\ \sigma_s^2 = \tau_s^2 \left(a_G^2 + b_G^2 \cos^2 E\right), \quad \tau_G : \tau_R : \tau_E : \tau_C = 1 : 1.5 : 2 : 2 \end{gathered} \tag{3}$$

where σ_s is the standard deviation of raw measurements (unit: m); E is the satellite elevation angle (unit: rad); a and b are empirical constants. For GPS, a and b are generally set to be 0.003 mm for carrier phase and 0.3 m for code observations. For GLONASS, Galileo and BDS, the coefficients are increased by a factor of 1.5, 2.0 and 2.0, respectively, due to the less accurate satellite orbit and clock products compared to GPS. In this study, the empirical weighting factors for different satellite systems are derived from numerous multi-GNSS PPP data processing by using variance component estimation method [21]. Firstly, multi-GNSS PPP is performed by using variance component estimation method, and then the empirical weighting factors for different satellite systems are obtained. Afterwards, the derived weight factors (approximately 1:1.5:2:2) are used in the subsequent real-time PPP processing.

The tropospheric slant total delay T_r^s consists of the hydrostatic and the wet components, both of which can be expressed by their individual zenith delay and mapping functions,

$$T_r^s = M_{h_r^s} \cdot Z_{h_r} + M_{w_r^s} \cdot Z_{w_r} \tag{4}$$

where $M_{h_r^s}$ and $M_{w_r^s}$ are the hydrostatic and wet coefficients of the global mapping function (GMF) [22]. The zenith hydrostatic delay (ZHD) Z_{h_r} can be computed by using the Saastamoinen model [23] and meteorological data, while the zenith wet delays (ZWD) Z_{w_r}, which commonly cannot be corrected well, have to be estimated as unknown parameters. In general, there is no need to estimate tropospheric gradient parameters for the RT ZTD estimation [24]. Additionally, to evaluate the impacts of different treatments of station positions, that is, fixed or estimated as kinematic, on the ZTD estimates, we calculate and make a comparison between the ZTDs derived from the two strategies.

A sequential least square filter is employed to estimate unknown parameters in RT processing. All the observations from different GNSS (four systems) are processed together in the common estimator to perform a rigorous multi-GNSS analysis with considering the inter-system and inter-frequency biases [8]. In RT multi-GNSS PPP based atmospheric parameter retrieving, the estimated parameters vector $\mathbf{X}$ can be expressed as,

$$\mathbf{X} = \left(Z_{w_r} t_r d_{rE} d_{rC} d_{rR_k} \mathbf{I}_{r,1}^s \overline{\mathbf{N}}_r^s\right)^T \tag{5}$$

$$\overline{\mathbf{N}}_r^s = \mathbf{N}_r^s + \mathbf{b}_r + \mathbf{b}^s \tag{6}$$

where the receiver clock bias t_r is estimated epoch-wise as white noise. The ISB and IFB parameters d_{rE}, d_{rC}, d_{rR_k} are estimated as constant over one processed day. The ionospheric delays $\mathbf{I}^s_{r,1}$ are taken as estimated parameters for each satellite at each epoch by using dual-frequency raw phase and pseudorange observations. The phase delays b_r and b^s will be absorbed by phase ambiguity parameters, and the phase ambiguities $\overline{\mathbf{N}}^s_r$ are estimated as constant for each continuous arc. The tropospheric ZWD Z_{w_r} is modeled as a random walk process and the noise intensity is about 5~10 $mm/\sqrt{h}$. The variance component estimation weighting method is also applied in this study. The multi-GNSS data processing strategies for retrieving RT tropospheric delays are summarized in Table 1.

Table 1. Processing strategies for the real-time (RT) multi-Global Navigation Satellite Systems (GNSS) zenith total delays (ZTD) estimation.

Item	Strategies
Estimator	All multi-GNSS observations are processed together in one sequential least square estimator.
Sources of satellite orbits & clocks	As shown in Table 2
Observations	Carrier phase and pseudorange observations; GPS + GLONASS + Galileo + BDS, about 80 navigation satellites
Signal selection	GPS: L1/L2; GLONASS: L1/L2; Galileo: E1/E5a; BDS: B1/B2
Sampling rate	5 s
Elevation cutoff	7°
Weight for observations	The variance component estimation weighting method
Satellite orbit	Fixed
Satellite clock	Fixed
Zenith Tropospheric delay	Initial model (ZHD estimated using Saastamoinen model based on GPT2) + random-walk process (process noise: 5 mm/h$^{1/2}$)
Tropospheric gradients	No
Mapping function	Global Mapping Function (GMF)
Phase-windup effect	Corrected
Receiver clock	Estimated, white noise
ISB and IFB	Estimated as constant, GPS as reference
Station displacement	Solid Earth tide, pole tide, ocean tide loading, IERS Convention 2010
Satellite antenna phase center	Corrected using MGEX and IGS values
Receiver antenna phase center	Corrected
Station coordinate	Fixed to coordinates of weekly solution/kinematic estimated
Phase ambiguities	Constant for each continuous arc, without ambiguity resolution

With Z_{h_r} and the estimated tropospheric parameter Z_{w_r}, the slant total delay can be reconstructed according to,

$$\widetilde{T}^s_r = M_{h^s_r} \cdot Z_{h_r} + M_{w^s_r} \cdot Z_{w_r} + \varphi \quad (7)$$

where $\widetilde{T}^s_r$ is the reconstructed slant total delay, φ denotes the post fit phase residual, which includes residual tropospheric delays due to the tropospheric asymmetry. In this study, pressure provided by the Global Pressure and Temperature 2 (GPT2) model is used to calculate the a priori ZHD so as to derive the ZTD (PPP-derived ZTD) [25].

3. Multi-GNSS Data and Products

3.1. Multi-GNSS Orbit and Clock Products from IGS RTS

In order to meet the requirements of RT GNSS precise applications, the IGS Real Time Working Group (RTWG) has officially provided the RT service (RTS) since 2013. The multi-GNSS orbit and clock products from RTS include precise orbit and clock corrections, which largely depend on the IGS infrastructure of the global RT network stations, the data centers, and the analysis centers that offer high-precision GNSS data products. To date, eight analysis centers are capable of providing the IGS-RT orbit and clock products, including BKG (Bundesamt für Kartographie und Geodäsie), CNES (Centre National d'Etudes Spatiales), DLR (Deutsches Zentrum für Luft- und Raumfahrt), ESA (European Space Agency), GFZ (Deutsches GeoForschungsZentrum), GMV (GMV Aerospace and Defense), and WUHAN (Wuhan University). Those analysis centers broadcast RT orbit and clock corrections through different mount points. Most of them provide GPS-only single-system or GPS/GLONASS dual-system RT orbit and clock products, while only a few analysis centers

(e.g., CNES and GFZ) are able to provide the GPS/GLONASS/Galileo/BDS four-system products. Table 2 lists the IGS-RT orbit and clock products from each analysis center in details.

Table 2. The International GNSS Service (IGS)-RT stream products from each analysis center.

IGS RTS	Reference Point	GNSS	Analysis Center
IGS01	APC	GPS	SE Combination
IGS02	APC	GPS	KF Combination
IGS03	APC	GPS/GLO	KF Combination
CLK70	APC	GPS	GFZ
CLK01	APC	GPS/GLO	BKG
CLK21	APC	GPS/GLO	DLR/GSOC
CLK16	APC	GPS	WUHAN
CLK81	APC	GPS/GLO	GMV
CLK92	CM	GPS/GLO/GAL/BDS	CNES
GFZC2	APC	GPS/GLO/GAL/BDS	GFZ
GFZD2	APC	GPS/GLO/GAL/BDS	GFZ

Currently, the RTS products, including the precise satellite orbit/clock corrections on the broadcast ephemeris, are distributed as the RT data streams (i.e., IGS01/IGC01, IGS02, and IGS03) and are expressed within the International Terrestrial Reference Frame 2008 (ITRF08). Additionally, the products can be accessed through internet without special licensing [26]. The accuracies for the orbits and clocks are 5 cm and 0.3 ns, respectively [27]. As an example, GFZ, as one of the IGS-RT data analysis centers, is able to offer the RT satellite orbit/clock products of all four systems to users with accuracy at cm level [14].

3.2. Multi-GNSS Data

The multi-GNSS Experiment (MGEX) [28] was initiated by IGS in 2012, to prepare for the incorporation of the new and modernized systems, which include Galileo, BDS, QZSS, and Navigation with Indian Constellation (NAVIC) systems, as well as the modernized GPS and the recovered GLONASS, and any other space-based augmentation system (SBAS) of interest [14]. A global multi-GNSS stations network, currently comprising more than 170 active stations, has been deployed under the framework of the MGEX campaign and integrated in parallel with the existing IGS network of GPS/GLONASS reference stations. As a minimum, all the MGEX stations support the tracking of GPS constellation as well as at least one of the new Galileo, BDS, or QZSS constellations, and the GLONASS satellites are tracked by most of the stations from MGEX. The majority of the MGEX stations allows for the RT data access in addition to the off-line archival data.

Meanwhile, various ACs and agencies have been providing the multi-GNSS products [29,30] and the satellite orbit/clock products for most of the new constellations have also been generated on a routine basis [31], which inspires much interest in using the multi-GNSS observations for PPP technique. The main supporters of MGEX are the CNES, Institut National de l'Information Géographique et Forestière (IGN), Geoscience Australia (GA), GFZ, Japan Aerospace Exploration Agency (JAXA), DLR, BKG, and the ESA, which contribute to roughly three quarters of the multi-GNSS stations. In early 2016, it was decided to terminate the experimental phase of the MGEX and to pursue IGS multi-GNSS activities as the "IGS Multi-GNSS Pilot Project". The term "MGEX" will be retained by IGS for this pilot project due to its high recognition achieved so far [32].

In this study, observational data of globally distributed MGEX stations are processed in operational RT PPP mode to retrieve the tropospheric delays. The geographic distribution of those stations along with their supporting constellations is illustrated in Figure 1.

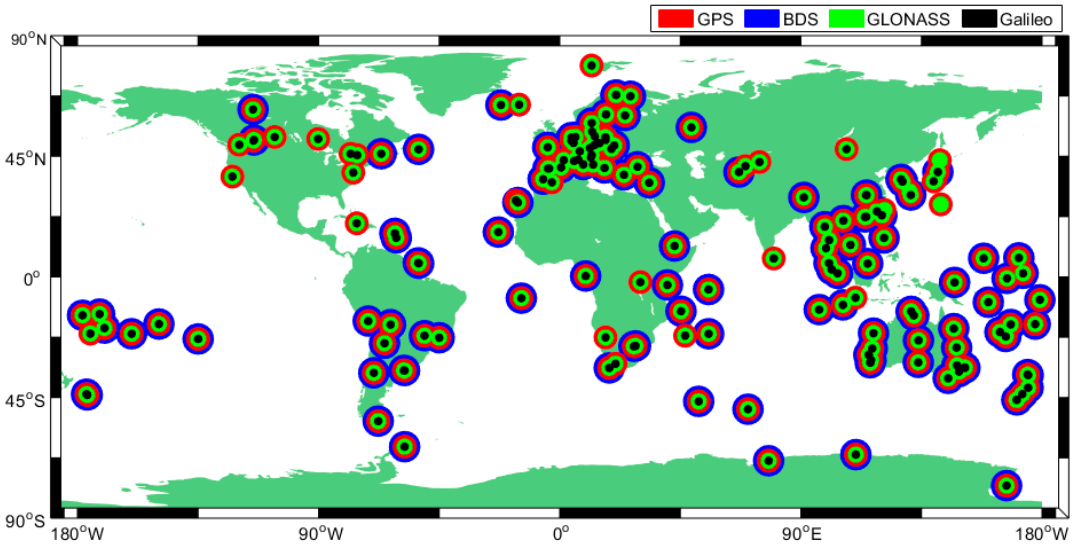

Figure 1. Geographical distribution of the multi-GNSS Experiment (MGEX) network and their supported navigation satellite constellations.

4. Results and Validations

4.1. Assessment of IGS-RT Orbit and Clock Products

As the performance of tropospheric delays derived from the multi-GNSS RT precise positioning depends on the accuracy and reliability of the employed RT precise orbit and clock products, the quality and capability of those products from different IGS RTS are evaluated before applied into the multi-GNSS processing. Here, taking the GFZ final orbit and clock products as reference, we analyze and compare different multi-GNSS RT orbit and clock products (i.e., CLK01, CLK81, CLK92, GFZC2 and GFZD2) over the period from day of year (DOY) 84 to DOY 101 in 2017. It is noteworthy that the four-system (GPS + GLONASS + Galileo + BDS) RT orbits and clocks are available from CLK92, GFZC2, and GFZD2, while CLK01 and CLK81 only support GPS and GLONASS products.

Figure 2 shows the RMS (root-mean-square) values of differences between the IGS-RT orbits and the GFZ final orbits for each satellite constellation in the along-track, cross-track, and radial components, respectively. The accuracy of RT GPS orbits is the best among all the orbital types in the three components, which is followed by GLONASS satellites. Limited to the insufficient number of globally tracking stations, the RT orbit accuracy for Galileo and BDS are not comparable to that for GPS or GLONASS. For the multi-GNSS orbits provided by the five ACs, the results in the radial component show a better agreement with the GFZ final orbits than those in the cross component, while the agreement in the along component is the worst.

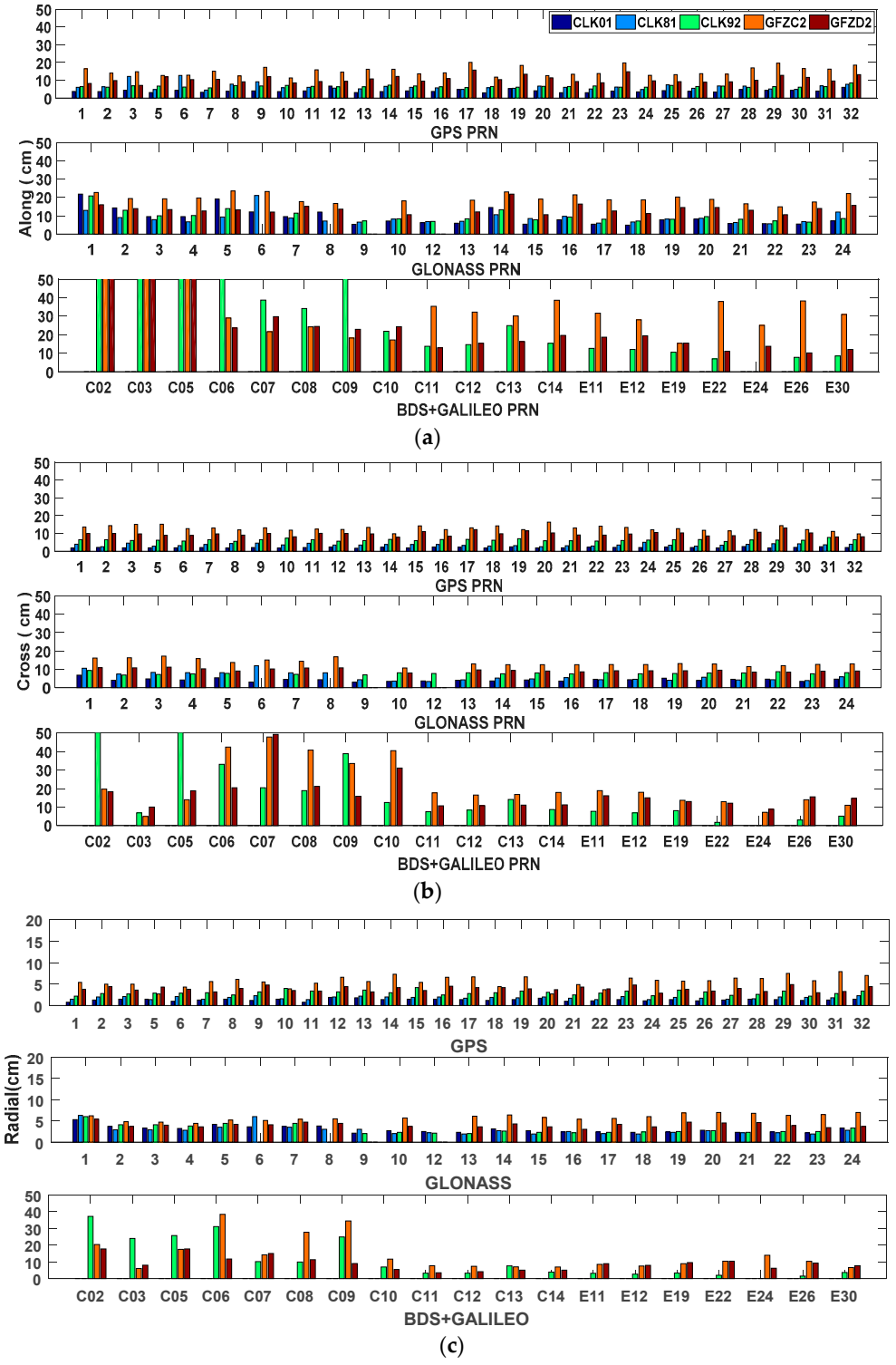

Figure 2. RMS (root-mean-square) values of the differences between IGS-RT orbits (CLK01, CLK81, CLK92, GFZC2, and GFZD2) and GeoForschungsZentrum (GFZ) final orbits for the four systems (i.e., Global Positioning System (GPS), Russian Global Navigation Satellite System (GLONASS), Galileo, and BDS) in the along (**a**), cross (**b**) and radial (**c**) components, respectively.

For GPS satellites, the RMS values for the CLK01 orbits that fit the best with the GFZ final orbits are less than 5 cm in the radial and cross components and below 10 cm in the along component. CLK81 provides slightly worse GPS orbits than CLK01 in particular for the along and cross components,

where the RMS values reach up to 12 cm and 7 cm, respectively. The CLK92 GPS orbit accuracy is very similar to that by CLK81 in the along and radial components, while the RMS value for CLK92 is about 11 cm in the cross component. In addition, the GPS RT orbits derived from GFZC2 and GFZD2 reveal lower accuracy than those from CLK01, CLK81, and CLK92. The RMS values for the GFZC2 GPS orbits can reach up to 25, 17, and 8 cm for the along, cross, and radial components, respectively.

The comparative results of the GLONASS satellite orbits derived from the different five ACs are similar to those of the GPS orbits mentioned above, except that they show a slightly lower accuracy than GPS orbits. For the RT GLONASS orbits, the RMS values for the CLK01 orbits are less than 20, 12, and 6 cm for the along cross, and radial, components, respectively, while the values for the GFZC2 orbits are about 22, 18, and 8 cm, respectively, in the three components.

The Galileo satellite orbits, offered by the CLK92, show a better agreement with the GFZ final orbits than those from other ACs. The RMS values for the CLK92 Galileo orbits are generally below 5 cm in the radial component, and less than 10 and 12 cm in the cross and along components. The RMS value for the GFZC2 orbits can reach about 38, 19, and 12 cm in the along, cross, and radial components, respectively.

For BDS GEO satellites (C01-05), the RT orbit products for the whole constellation cannot be continuously provided by CLK92, GFZC2 and GFZD2 since the corresponding global distribution of GEO tracking stations are not good and the data streams for some of the satellites are always missing, such as for satellites C01 and C03. For BDS inclined geosynchronous orbit (IGSO) (C06-10) satellites, the orbits provided by GFZD2 reveal the best accuracy in all three components. The CLK92 orbits show the lowest accuracy in the along component, and the GFZC2 orbit accuracy is the worst in the cross and radial components. For BDS medium earth orbit (MEO) (C11-14) satellites, CLK92 and GFZD2 offer the RT orbits with similar accuracy, better than the GFZC2 ones. The RMS values for the CLK92 orbits are within 23, 15, and 7 cm in the along, cross, and radial components, respectively, which are no more than 38, 19, and 14 cm, respectively for the GFZC2 orbits.

Figure 3 shows the averaged RMS values of the differences between IGS-RT orbits and GFZ final orbits for GPS, GLONASS, Galileo, and BDS satellites in the along, cross, and radial components, respectively. It can be seen that CLK01 provides the highest accuracy of both GPS and GLONASS satellite orbits. The averaged RMS values for the CLK01 GPS orbits are about 4.00, 2.12, and 1.34 cm in the along, cross, and radial components, respectively, which are about 9.15, 4.30, and 2.99 cm for the CLK01 GLONASS orbits. The GPS and GLONASS orbits offered by CLK81 show similar accuracy with those offered by CLK92, and they are both less accurate than the CLK01 orbits. The GPS and GLONASS orbits obtained from GFZC2 show the lowest accuracy. The averaged RMS values for GPS are 15.13, 12.92, and 5.61 cm in along, cross, and radial components, respectively, and for GLONASS they are 9.50, 13.67, and 5.85 cm.

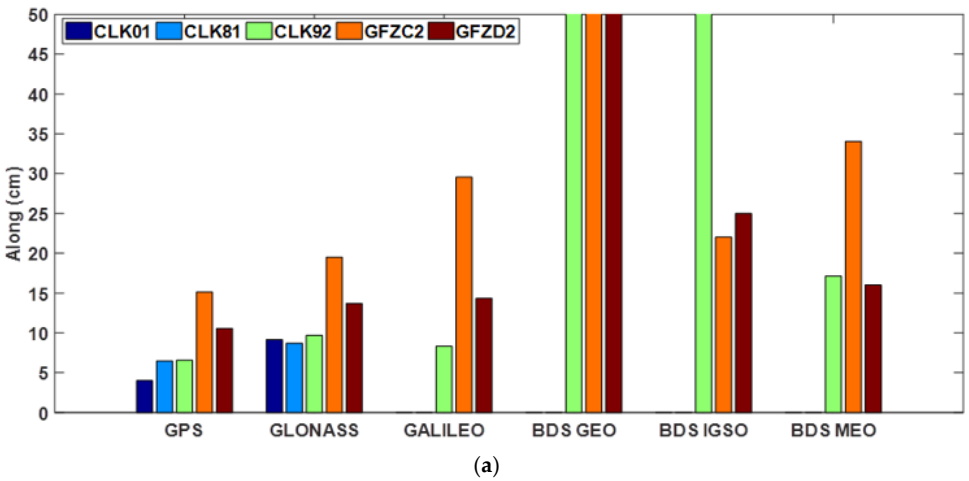

(**a**)

Figure 3. *Cont.*

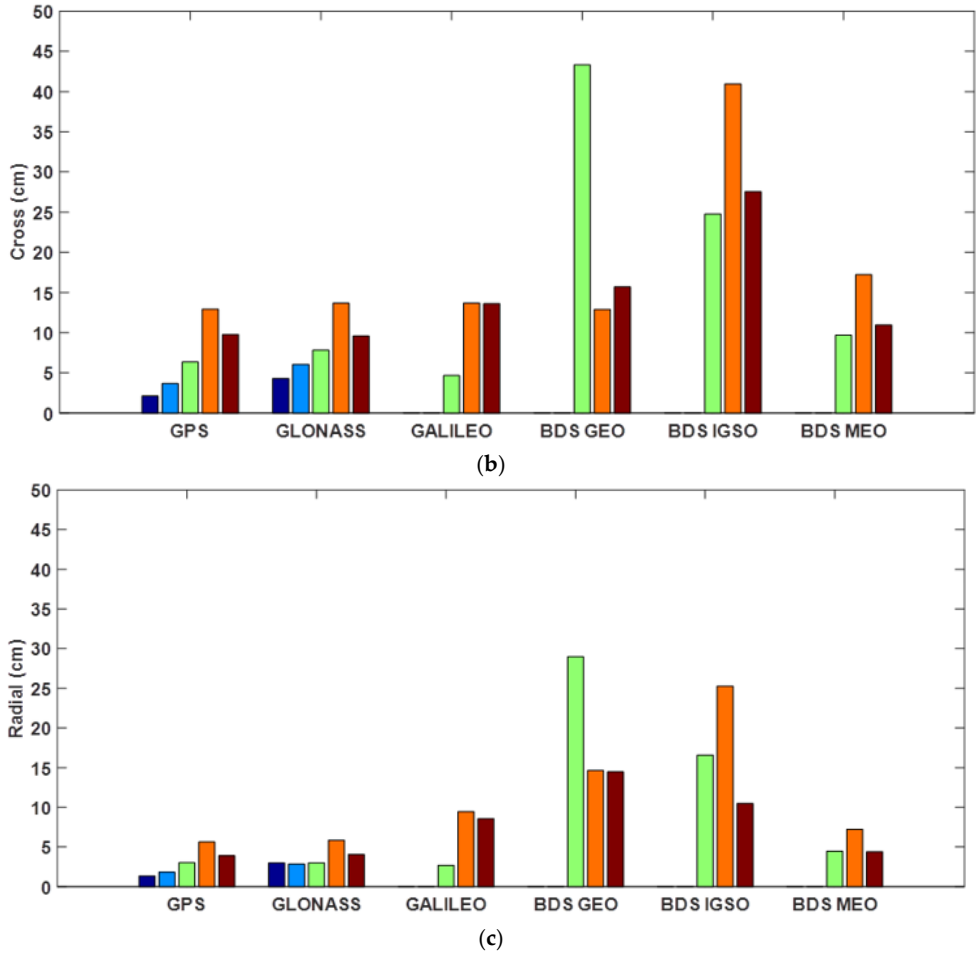

Figure 3. Averaged RMS values of the differences between IGS-RT orbits and GFZ final orbits for GPS, GLONASS, Galileo, and BDS satellites in the along (**a**), cross (**b**), and radial (**c**) components, respectively.

The Galileo orbits from CLK92 show a better accuracy of 8.31, 4.66, and 2.68 cm in the three components, respectively, compared to those from GFZC2 and GFZD2. For BDS satellites, the orbit accuracy of BDS GEO satellites is much lower than that of IGSO and MEO. This could be due to the fact that the GEO satellites do not move significantly with respect to the ground stations, resulting in a rather weak geometrical constellation. Meanwhile, low elevation of the satellites' signals tracked at several stations far away from Asia-Pacific region and constant multipath error also have negative impact on orbit accuracy. Currently, the RT GEO orbits derived from any ACs are not reliable. The GFZD2 offer the best orbit accuracy of BDS IGSO satellites, where the averaged RMS values are about 24.98, 27.54, and 10.48 cm in the along, cross, and radial components, respectively. The accuracy of BDS MEO satellite orbits offered by CLK92 is comparable to that by GFZD2. The CLK92 MEO orbits reveal averaged accuracies of 17.13, 9.68, and 4.48 cm in the three components, respectively, while the accuracies for the GFZD2 MEO orbits are about 34.05, 17.23, and 7.23 cm, respectively. The averaged RMS values of the differences between IGS-RT orbits and GFZ final orbits for the four systems are also summarized in Table 3.

Table 3. The averaged RMS values of the differences between IGS-RT orbits and GFZ final orbits for GPS, GLONASS, Galileo, and BDS.

IGS-RT Service	TYPE	Along (cm)	Cross (cm)	Radial (cm)
CLK01	GPS	4.00	2.12	1.34
	GLONASS	9.15	4.30	2.99
CLK81	GPS	6.46	3.65	1.83
	GLONASS	8.70	6.06	2.83
CLK92	GPS	6.54	6.34	3.00
	GLONASS	9.69	7.81	2.99
	Galileo	8.31	4.66	2.68
	BDS GEO	59.79	43.33	28.97
	BDS IGSO	50.22	24.74	16.58
	BDS MEO	17.13	9.68	4.48
GFZC2	GPS	15.13	12.92	5.61
	GLONASS	19.50	13.67	5.85
	Galileo	29.56	13.67	9.44
	BDS GEO	65.83	12.90	14.63
	BDS IGSO	22.02	40.96	25.28
	BDS MEO	34.05	17.23	7.23
GFZD2	GPS	10.56	9.77	3.89
	GLONASS	13.68	9.57	4.04
	Galileo	14.31	13.60	8.56
	BDS GEO	60.37	15.70	14.47
	BDS IGSO	24.98	27.54	10.48
	BDS MEO	16.00	10.95	4.40

Afterwards, the GFZ final clock products are employed as reference to assess the quality of the multi-GNSS RT clocks offered by CLK01, CLK81, CLK92, GFZC2, and GFZD2. In general, the standard derivation (STD) is equal to the RMS since the removed mean biases can be absorbed by ambiguity items. Here, the STD value will be taken as the indicator for evaluating the clock quality. The STD values of the differences between the IGS-RT clocks and the GFZ final clocks for the four systems (i.e., GPS, GLONASS, Galileo, and BDS) are illustrated in Figure 4.

As can be seen from Figure 4, the RT GPS satellite clocks agree well with the GFZ final clocks, in particular for those provided by CLK92, whose STD values are generally less than 0.15 ns. The clock accuracies of GPS satellites are around 0.2 ns for the CLK01 and CLK82, while GFZC2 and GFZD2 provide the RT GPS clocks with the accuracy of about 0.3 ns. For GLONASS satellites, the STD values of the difference between RT CLK01 clocks and the GFZ final clocks are 0.22 ns or so, which is the best among those RT GLONASS clocks. The STD values for CLK92 GLONASS clocks range from 0.3 to 0.4 ns, while those for GFZC2 and GFZD2 clocks are between 0.2 and 0.4 ns. Additionally, the accuracy of RT GLONASS satellite clocks provided by CLK81 is comparable to that by CLK92.

The Galileo clocks derived from CLK92 provide a higher accuracy of between 0.1 and 0.25 ns than those of around 0.5 ns from GFZC2 and GFZD2. The STD value for BDS GEO satellite clocks from CLK92 can reach about 0.4 ns. For BDS IGSO and MEO satellites, a better clock accuracy of 0.2 to 0.6 ns can be obtained for GFZD2 compared to those for CLK92 and GFZC2.

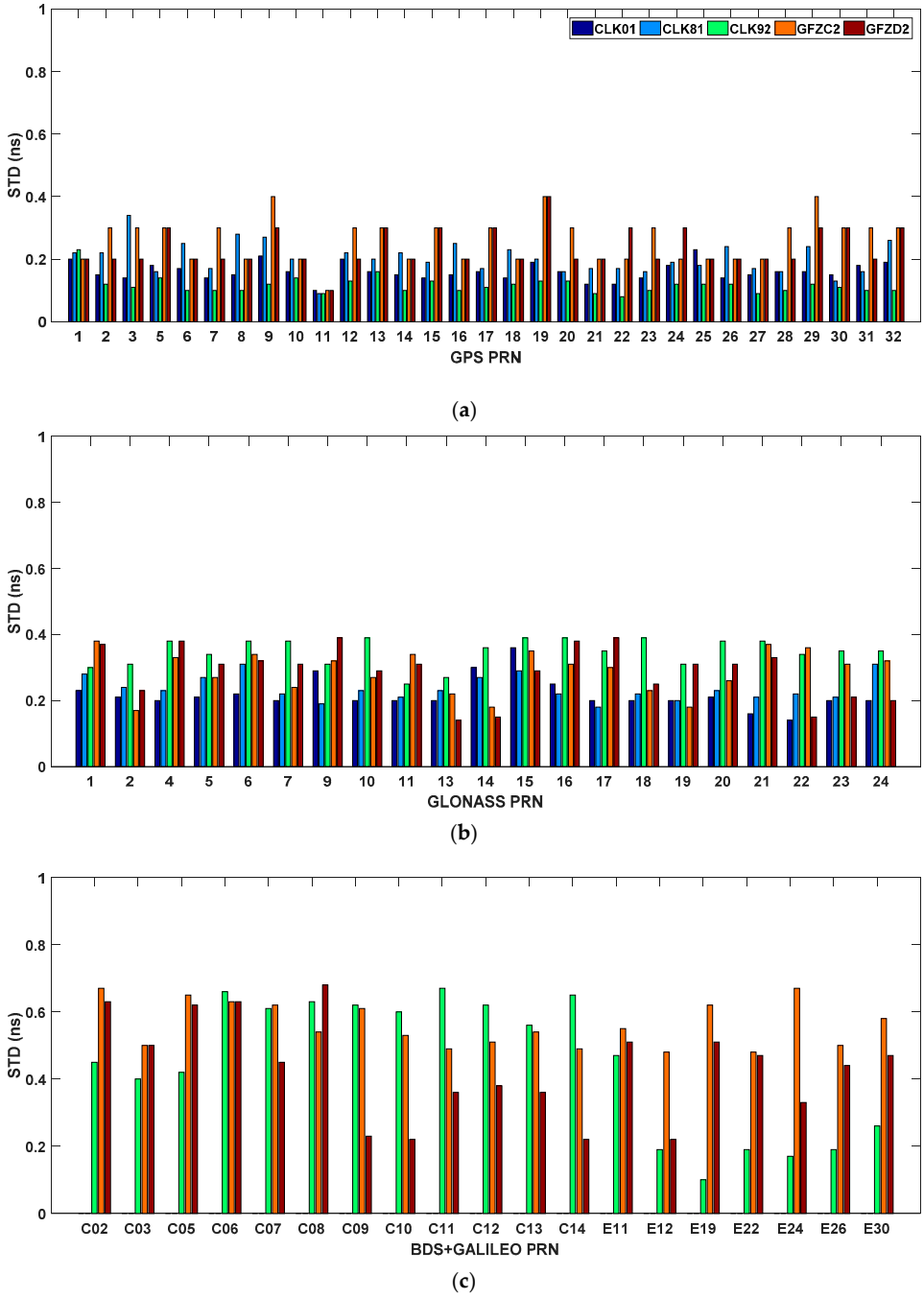

Figure 4. STD values of differences between IGS-RT clocks and the GFZ final clocks for each satellite from GPS (**a**), GLONASS (**b**), BDS and Galileo (**c**).

Figure 5 illustrates the averaged STD values of the differences between the IGS-RT clocks and the reference clocks for each system. In general, the GPS clocks fit the best with the GFZ final clocks, while the GLONASS clocks reveal a slightly worse agreement. Compared to RT GLONASS clocks, the relatively lower clock accuracy for Galileo and BDS could be attributed to the currently uncompleted constellation, as well as the limited number of available tracking stations. However, the quality of the BDS and Galileo products is expected to be improved in the future with more satellites in orbit, a more densified tracking network, and the enhanced availability of more accurate parameters in the space segment [32].

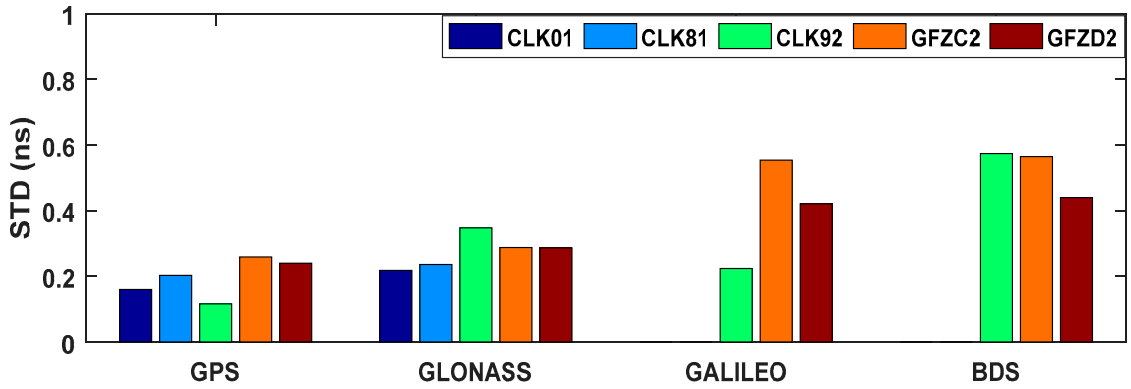

Figure 5. The averaged STD values of the differences between the IGS-RT clocks and the reference for GPS, GLONASS, Galileo, and BDS.

For GPS satellites, the RT clocks offered by CLK92 show the highest accuracy, while those by GFZC2 and GFZD2 present the worst accuracy. The averaged STD values of all GPS satellites are about 0.16, 0.20, 0.12, 0.26 and 0.24 ns for CLK01, CLK81, CLK92, GFZC2 and GFZD2, respectively. For the GLONASS satellites, the averaged STD values for CLK01 and CLK81 clocks are about 0.22 and 0.24 ns, respectively, while the GLONASS clocks provided by CLK92 reveal an averaged STD of 0.35 ns. The accuracies for both the GFZC2 and GFZD2 GLONASS clocks are about 0.29 ns.

As for the Galileo satellites, the CLK92 clocks achieve a higher accuracy compared to GFZC2 and GFZD2. The averaged accuracies are about 0.22, 0.55, and 0.42 ns for the CLK92, GFZC2, and GFZD2 clocks, respectively. For the BDS satellites, the clocks derived from GFZD2 show the best accuracy in comparison with those from CLK92 and GFZC2. The averaged STD values of all BDS satellites are about 0.57, 0.56, and 0.44 ns for the CLK92, GFZC2, and GFZD2 clocks, respectively.

In summary, the quality of real-time products provided by these RT services is different from each other. This may be related to the different processing strategies and different observation streams of real-time precise orbit determination (POD) and precise clock estimation (PCE) adopted by various analysis centers. They are improving their models and strategies for better quality of real-time products.

4.2. ZTD Validation with the Final Tropospheric Products

Based on the IGS-RT multi-GNSS orbit and clock products, the operational RT ZTD can be retrieved. In this section, we investigate and compare the impact of different systems, different multi-GNSS combination and different positioning modes (i.e., fixing coordinate and kinematic modes) on the performance of the multi-GNSS RT ZTD estimates [8]. By processing observation data from the selected 30 tracking stations equipped with the four-system receivers as described in Section 2, the RT ZTD estimates are obtained every five seconds during the time period from March 28 to April 11 2017. The final troposphere products provided by the U.S. Naval Observatory (USNO) are taken as the reference data sets here. The USNO products with the sampling rate of five minutes are generated by using PPP with the IGS final orbit/clock products [33].

Figure 6 shows the RT ZTD results at station ONS1 (Onsala, Sweden, 57.39° N, 11.92° E) for different IGS-RT services with processing the GPS-only, the combined GPS/GLONASS, and the combined GPS/GLONASS/Galileo/BDS observations in fixing coordinate and kinematic processing modes over the first two hours of DOY 090, 2017. From Figure 6, we can clearly see that, for either fix coordinate or kinematic positioning mode, there is no big difference between the RT ZTDs derived from different IGS-RT services after 40 min, no matter which of the multi-GNSS combination are employed.

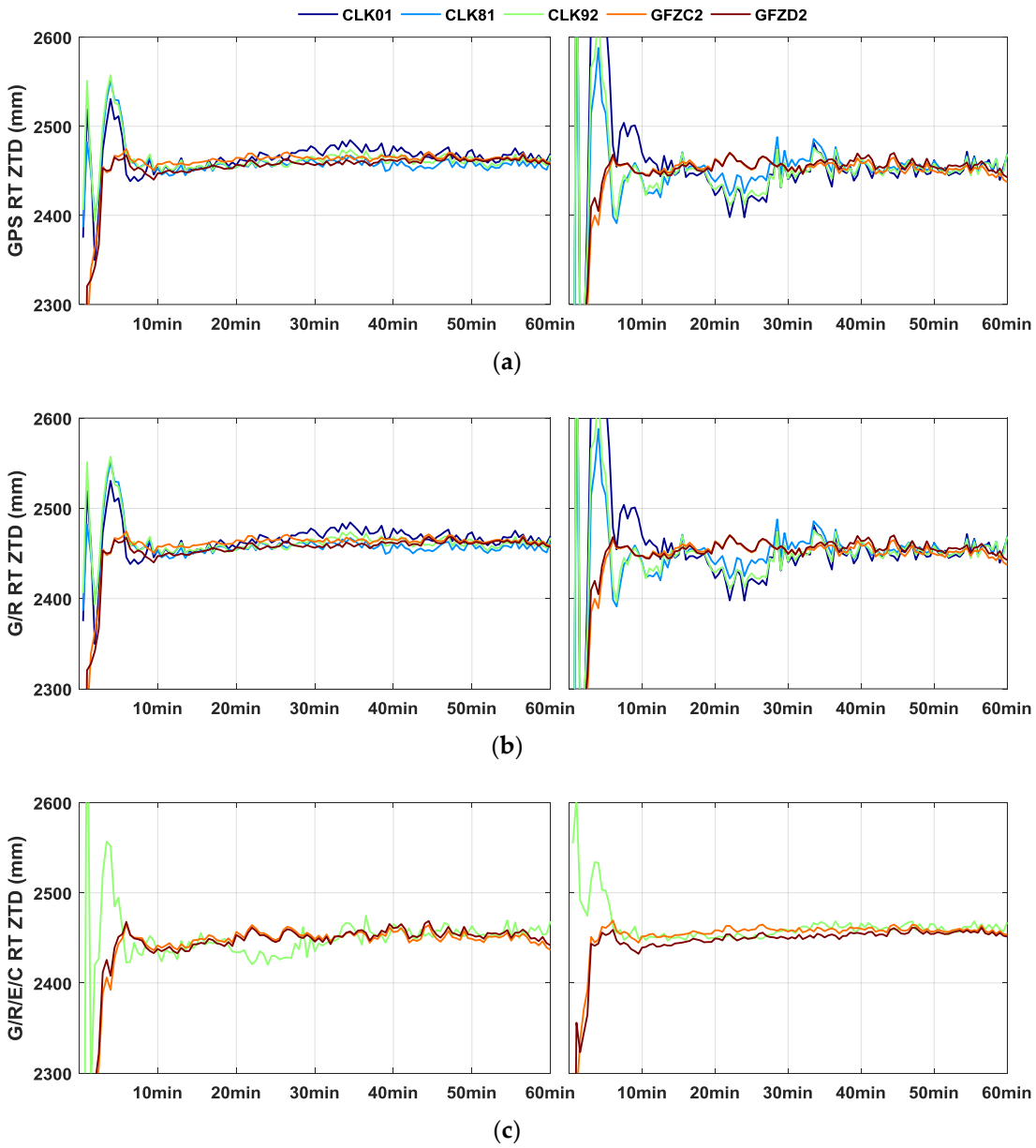

Figure 6. RT ZTD estimates at station ONS1 derived from the GPS-only ("GPS", **a**), the combined GPS/GLONASS ("G/R", **b**), and the combined GPS/GLONASS/Galileo/BDS ("G/R/E/C", **c**) solutions in fixing coordinate (left panels) and kinematic processing (right panels) modes by employing different IGS-RT service over the first 2 h of DOY 090, 2017.

In the GPS-only solution with fixinTg the coordinates, the shortest convergence time of less than five minutes for RT ZTD estimates can be achieved by GFZC2 and GFZD2 compared to that of about eight minutes for other IGS-RT services [8]. In contrast, the results in the kinematic mode exhibit longer convergence period and worse stability than those in the fixing coordinate mode. For example, the initial convergence time of RT ZTDs for GFZC2 and GFZD2 in the kinematic mode is about ten minutes. With introducing more GNSS observations, the performance of ZTD estimates can be improved in the combined GPS/GLONASS and GPS/GLONASS/Galileo/BDS solutions compared to the GPS-only one, especially for the convergence time in kinematic positioning mode. Similar to the GPS-only case, the GFZC2 and GFZD2 provide the best results of RT ZTDs in the combined solutions.

By using different IGS-RT service and different combination of multi-GNSS observations in the fixing coordinate mode, we provide the averaged initial convergence time of RT ZTDs for all

stations as summarized in Figure 7. The initialization process is considered to be completed when the differences between the estimated RT ZTDs and the post-processed USNO ZTDs become and remain smaller than a given value, which is set to be 20 mm here following the mean of the threshold and goal value of ZTD for weather nowcasting [34]. With the increased number of observations, the initialization time for the dual-system combination (GPS/GLONASS) and the four-system combination (GPS/GLONASS/Galileo/BDS) become shorter than that for the single-system solution (GPS-only). In addition, the results for GFZC2 and GFZD2 outperform those for the other three services (i.e., CLK01, CLK81, and CLK92) in each solution. Based on the GFZC2 products, the averaged initialization time of RT ZTDs can reach about 522 s (8.7 min), 492 s (8.2 min), and 480 s (8.0 min) in the GPS-only, dual-system (GPS/GLONASS), and the four-system (GPS/GLONASS/Galileo/BDS) solutions, respectively. Compared to the GPS-only solution, the initialization time for GFZC2 can be improved by about 5.8% and 8.1% with the dual-system and the four-system combinations, respectively. The averaged initialization time for the CLK92 RT products are 570 s (9.5 min), 522 s (8.7 min), and 510 s (8.5 min) for the GPS-only, the combined GPS/GLONASS, and the combined GPS/GLONASS/Galileo/BDS solutions, respectively, and the improvements of the dual-system and the four-system combined solutions to the GPS-only solution are about 8.4% and 10.5%, respectively. The averaged initialization time for different IGS-RT service in the single-system, the dual-system, and the four-system solutions with fixing coordinate are listed in Table 4.

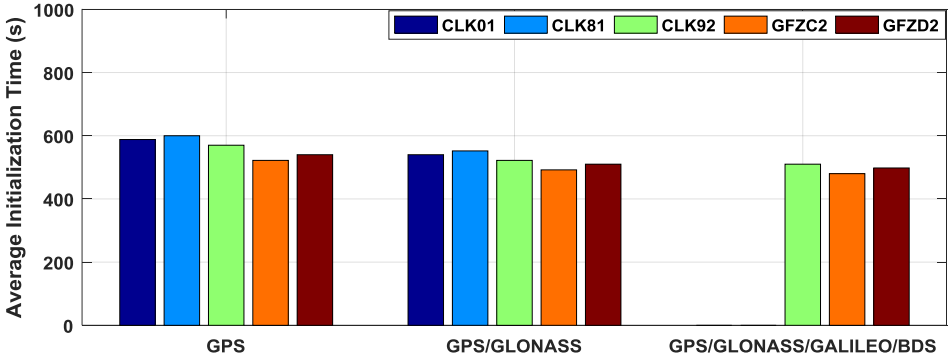

Figure 7. Averaged initialization time for all stations from the GPS-only, the combined GPS/GLONASS, and the combined GPS/GLONASS/Galileo/BDS four-system solutions with different IGS-RT service in the fixing coordinate modes.

Table 4. Averaged initialization time (unit:s) for different IGS-RT service from the single-system, the dual-system, and the four-system solutions in the fixing coordinate mode.

Solution	CLK01 (s)	CLK81 (s)	CLK92 (s)	GFZC2 (s)	GFZD2 (s)
GPS	588	600	570	522	540
GPS/GLONASS	540	552	522	492	510
GPS/GLONASS/Galileo/BDS	-	-	510	480	498

In order to evaluate the accuracy of RT ZTD estimates, their differences between the USNO final ZTD values are taken into account at each common epoch after the convergence. This will avoid the potential errors caused by the temporal interpolation of troposphere products. By processing GNSS observations on DOY 090, 2017 in the fixing coordinate mode, the accuracy of the estimated RT ZTDs derived from the five RT services are illustrated in Figure 8 for the GPS-only, the combined GPS/GLONSS, and the combined GPS/GLONASS/Galileo/BDS solutions, respectively.

In the case of GPS-only, the results for CLK81 show the largest deviations with respect to the USNO final ZTD, which is followed by those for GFZD2. The CLK01 results agree slightly better with the final ZTD, compared to the CLK81 ones, while the best agreement can be obtained based

on the GFZC2 products, with less noise and fewer outliers. In the combined GPS/GLONASS and GPS/GLONASS/Galileo/BDS solutions, the GFZC2 results also agree the best with the USNO final ZTD, followed by CLK92, while the GFZD2 results reveal the largest deviations. Besides, a better agreement between the improved ZTD estimates and the reference values can be achieved in the combined GPS/GLONASS/Galileo/BDS ZTDs compared to the GPS-only ZTDs, which confirms the superiority of multi-GNSS again. Figure 9 illustrates the comparison between the RT ZTD and the USNO final ZTD products at station ONS1 in the kinematic mode for the single-, dual-, and four-system solutions. Compared to the fixing coordinate mode, the RT ZTD estimates in the kinematic mode present much larger deviations and more noise with respect to the final ZTD.

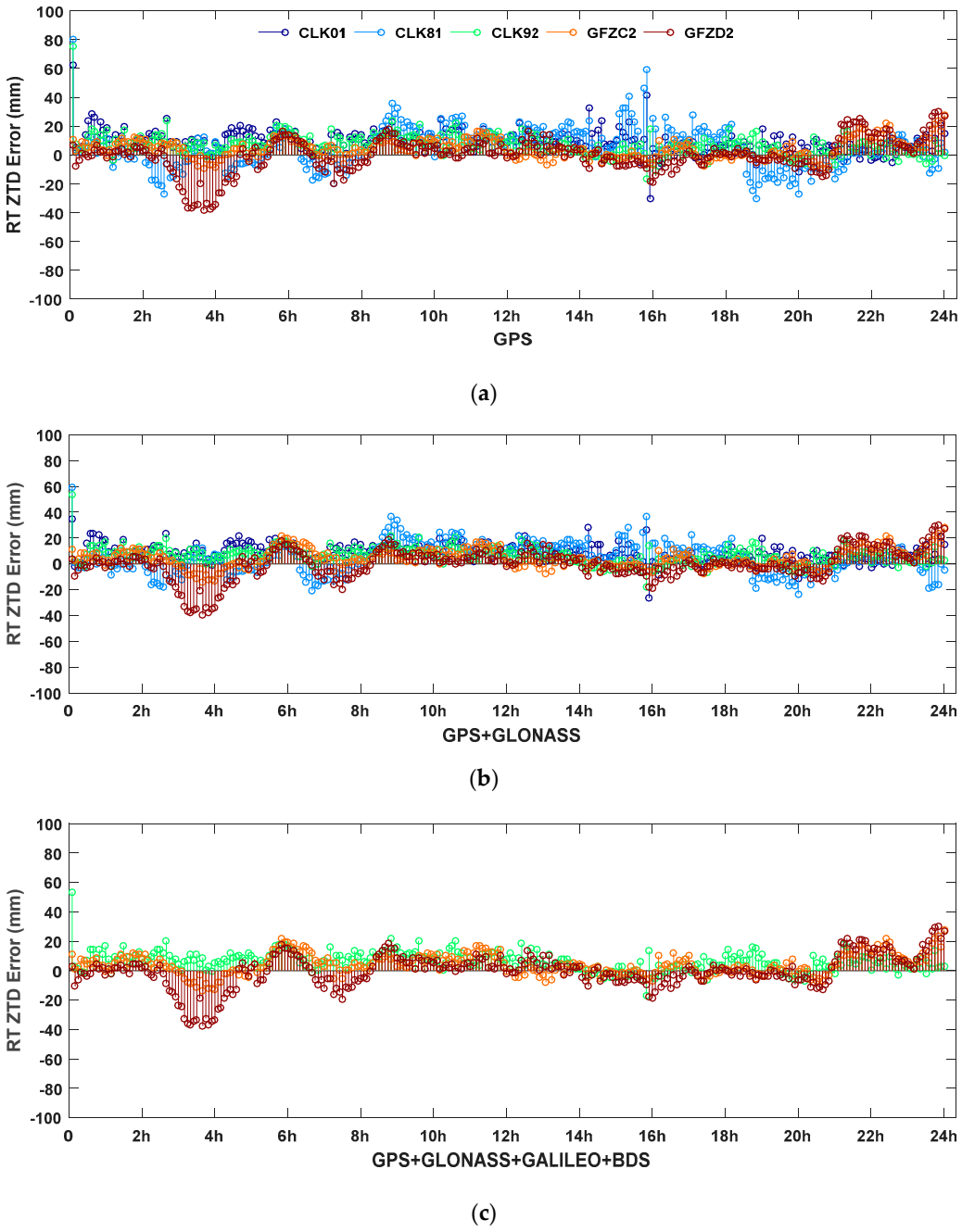

(**a**)

(**b**)

(**c**)

Figure 8. Differences of the RT ZTD in the fixing coordinate mode, derived from the GPS-only (**a**), the combined GPS/GLONSS (**b**), and the combined GPS/GLONASS/Galileo/BDS (**c**) solutions, with the USNO final troposphere products on DOY 090, 2017 at station ONS1.

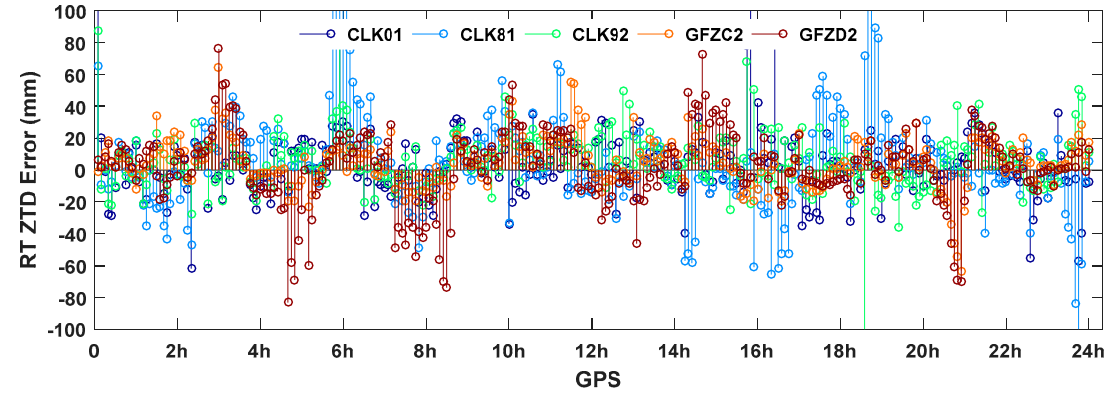

(**a**)

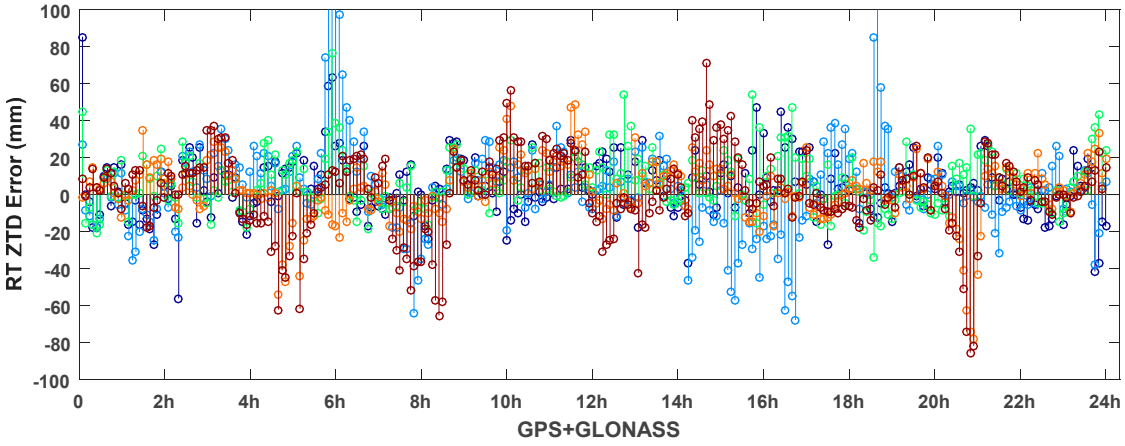

(**b**)

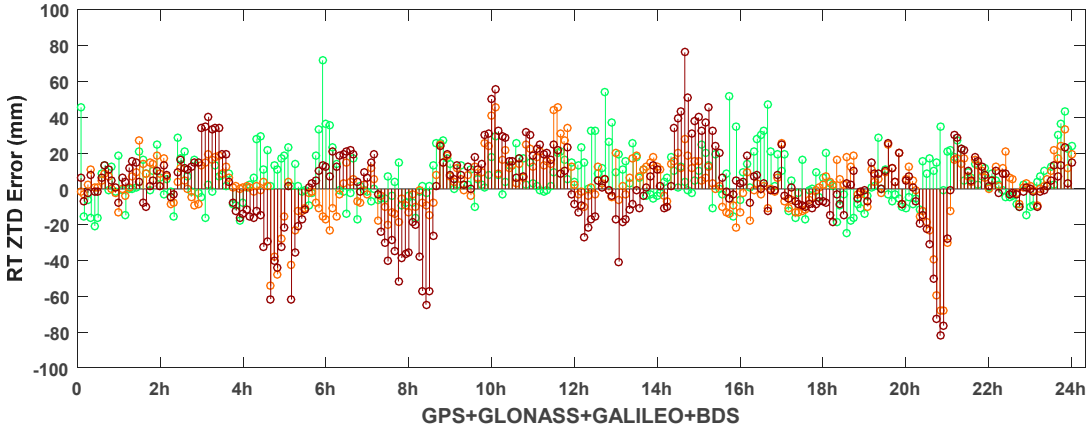

(**c**)

Figure 9. Differences of the RT ZTD in the kinematic mode, derived from the GPS-only (**a**), the combined GPS/GLONSS (**b**), and the combined GPS/GLONASS/Galileo/BDS (**c**) solutions, with the USNO final troposphere products on DOY 090, 2017 at station ONS1.

The RMS values of the ZTD differences from the three solutions in the fixing coordinate and the kinematic modes with respect to the USNO final tropospheric products at station ONS1 on DOY 092, 2017 are shown in Figure 10. Generally, the RT ZTDs retrieved in the fixing coordinate mode show much

higher accuracy in comparison with those in the kinematic mode. Besides, better ZTD estimates can be achieved in the combined GPS/GLONASS and GPS/GLONASS/Galileo/BDS solutions, compared to the GPS-only solution. As mentioned previously, the GFZC2 provides the best RT ZTD results for all the three solutions in both fixing coordinate and kinematic modes. In the fixing coordinate mode, the RMS value for the GPS-only solution is about 7.9 mm, while the values are about 7.5 mm and 7.3 mm for the combined GPS/GLONASS and the combined GPS/GLONASS/Galileo/BDS solutions, respectively. However, the RMS values for the three solutions are much larger in the kinematic mode, which are about 16.5, 15.0, and 15.1 mm, respectively.

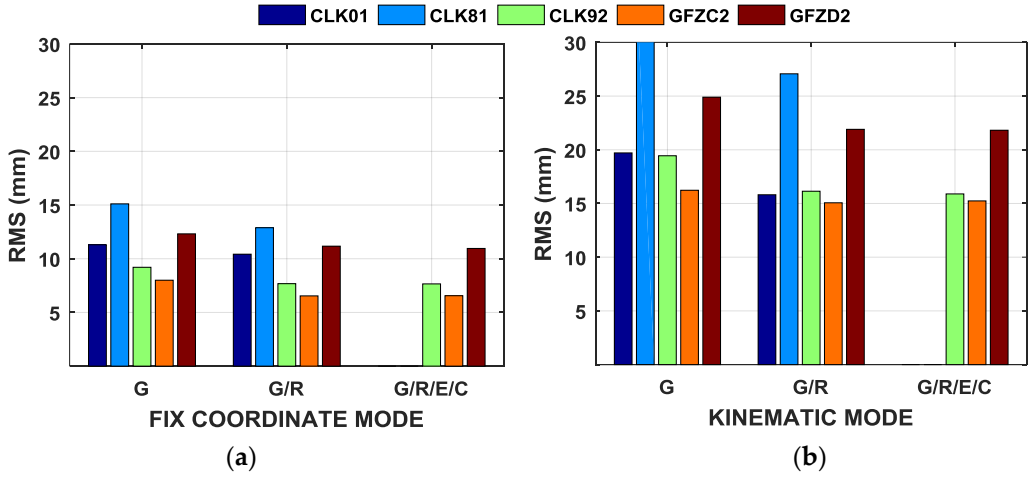

Figure 10. RMS values of the ZTD differences from the GPS-only ("G"), the combined GPS/GLONASS ("G/R"), and the combined GPS/GLONASS/Galileo/BDS ("G/R/E/C") solutions in the fixing coordinate (**a**) and the kinematic (**b**) modes with respect to the USNO final tropospheric products at station ONS1 on DOY 092, 2017.

Figure 11 presents the averaged RMS of the RT ZTD differences for all stations during the whole period (DOY 84-101, 2017) in both the fixing coordinate and the kinematic modes. Generally, the RT ZTDs retrieved in the fixing coordinate mode show much higher accuracy compared to those in the kinematic mode and the advantage of multi-GNSS is also obvious in this case. Compared to the other IGS-RT service, the RT ZTD of GFZC2 shows the highest accuracy for each solution in both the fixing coordinate and the kinematic modes. The averaged RMS values of GFZC2 ZTDs are about 6.50, 5.04, and 5.06 mm in the fixing coordinate mode for the GPS-only, the combined GPS/GLONASS, and the combined GPS/GLONASS/Galileo/BDS solutions and about 14.73, 13.57, and 13.74 mm in the kinematic mode. Consequently, the improvement in the accuracy of the real-time estimated ZTDs can reach about 22.2% due to introducing multi-GNSS observables compared to the GPS-only solution. For the multi-GNSS real-time retrieving tropospheric delays, the ZTD accuracy in the fixing coordinate mode can be improved by a factor of approximately 2.7 in comparison to that in the kinematic mode. The RMS values of the CLK81 ZTD estimates for the GPS-only and the combined GPS/GLONASS solutions are about 13.61 and 11.39 mm, respectively, in the fixing coordinate mode, and about 33.50 and 25.57 mm, respectively, in the kinematic mode. In the combined GPS/GLONASS/Galileo/BDS solution, the RMS values for the GFZD2, CLK92 and GFZC2 RT ZTDs are about 9.46, 6.16, and 5.06 mm, respectively, in the fixing coordinate mode, and about 20.32, 14.39, and 13.74 mm, respectively, in the kinematic mode. The related RMS statistics are listed in Table 5.

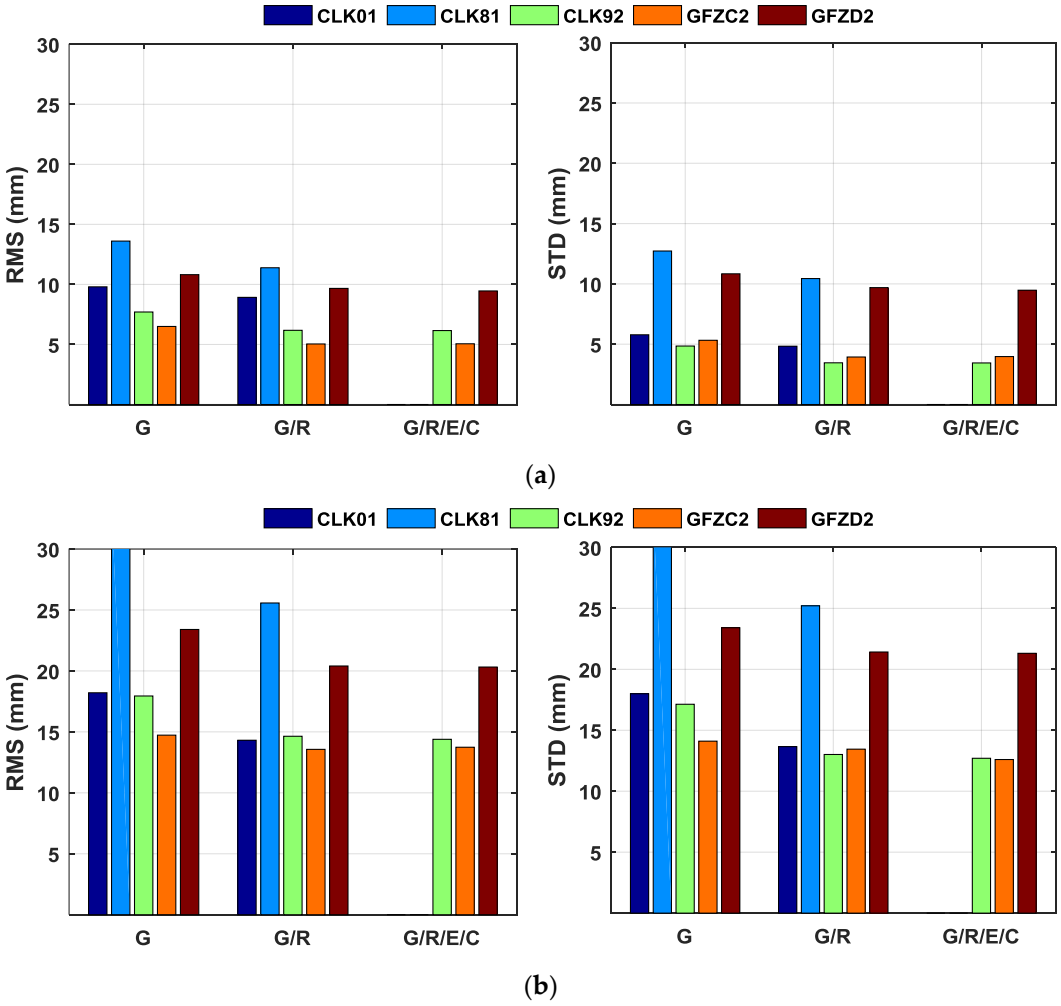

Figure 11. Averaged RMS and STD values of the RT ZTD differences for all stations during the whole period (DOY 84-101, 2017) in both the fixing coordinate (**a**) and the kinematic modes (**b**).

Table 5. Statistical results of the RT ZTD differences for the fixing coordinate and the kinematic modes (unit: mm).

IGS Service	Solution	Fix Coordinate Mode		Kinematic Mode	
		RMS	STD	RMS	STD
CLK01	G	9.80	5.78	18.21	18.00
	G/R	8.92	4.83	14.31	13.66
CLK81	G	13.61	12.73	33.50	32.97
	G/R	11.39	10.44	25.57	25.21
CLK92	G	7.70	4.85	17.94	17.13
	G/R	6.18	3.46	14.64	13.01
	G/R/E/C	6.16	3.45	14.39	12.70
GFZC2	G	6.50	5.32	14.73	14.11
	G/R	5.04	3.94	13.57	13.45
	G/R/E/C	5.06	3.97	13.74	12.60
GFZD2	G	10.81	10.84	23.40	23.41
	G/R	9.67	9.69	20.40	21.42
	G/R/E/C	9.46	9.48	20.32	21.32

5. Discussion

With the rapid development of GNSS, more researchers have been investigating its applications in meteorology. Most of these previous studies only involve both post-processing and near-RT modes [4–6]. However, sufficient information of the atmosphere state should be delivered with short or even no latency for some innovative applications, such as nowcasting and short-term weather forecasting. Different from previous studies, we focus on the actual real-time retrieving of tropospheric delays in this paper. To achieve this, the real-time satellite clock and orbit products and multi-GNSS data streams are required. In Section 4.1, we assessed the quality of the real-time products derived from various operating IGS services. As shown in Figures 3 and 5, the real-time orbit and clock accuracies for emerging BDS and Galileo satellites are still not comparable to those for GPS and GLONASS satellites. Moreover, the lower accuracy of Galielo and BDS ephemerides doses not directly translate to ZTD results, what is seen in Table 5 where the results for G/R and G/R/E/C are very similar. The qualities of real-time products for BDS and Galileo are expected to be further improved with the setup of more GNSS tracking ground stations in the future.

Based on real-time orbit and clock products and data streams, the real-time tropospheric parameters can be estimated by using the real-time PPP technology. In Section 4.2, we evaluate the accuracy of real-time ZTDs comparing with the final tropospheric products for the different solutions. The results confirm that the performance of real-time retrieving tropospheric delays can be improved due to the fusion of multi-GNSS compared to the single-system constellation. In addition, we also demonstrate that the fixing coordinate mode is more suitable for extracting real-time ZTD estimates based on real-time products derived from different IGS-RT services. In the multi-GNSS solution, the ZTD accuracy in the fixing coordinate mode can be improved by a factor of approximately 2.7 in comparison to that in the kinematic mode.

With the launch of more new satellites and setup of more ground GNSS stations, the quality of real-time orbit and clock products provided by IGS-RT services will be improved, especially for BDS and Galileo. Consequently, the real-time retrieved ZTDs with higher accuracy can be achieved by using multi-GNSS real-time PPP technology.

6. Conclusions

In this study, we at first assessed the accuracy of the multi-GNSS orbit and clock solutions from different IGS-RT services, comparing with GFZ final orbit and clock products. Then, we fully exploited the available multi-GNSS observations to validate the method of RT atmospheric parameter retrieving based on different IGS-RT orbit and clock services. Furthermore, we have conducted a detailed analysis of the initialization time and accuracy of the retrieved RT ZTD estimates by using the USNO products as a reference.

In terms of the accuracy of RT orbits, the results show that for the GPS satellites, the RMS values of the differences between IGS-RT orbits and GFZ final orbits are generally better than 5 cm in radial and cross-track directions, and better than 10 cm in along-track direction. For the GLONASS satellites, the RMS values are generally better than 8 cm in radial and cross-track directions, and better than 12 cm in along-track direction which is slightly worse than the GPS orbit accuracy. For the BDS IGSO satellites, GFZD2 has the best orbit accuracy, for the BDS MEO satellites, CLK92 and GFZD2 have comparable orbit accuracies, better than that for GFZC2. Additionally, the results for the RT clocks show that the GPS clock has the highest accuracy comparing with the other system clocks. CLK92 has the highest GPS clock accuracy which is about 0.12 ns. CLK01 has the highest GLONASS clock accuracy which is about 0.22 ns. CLK92 has the highest Galileo clock accuracy which is about 0.22 ns. GFZD2 has the highest BDS clock accuracy which is about 0.44 ns.

As for the RT ZTD estimates, the results reveal that the initialization process can be accelerated in the fixing coordinate mode comparing with that in the kinematic positioning mode. By fully exploiting multi-GNSS observables, the convergence time of the real-time estimated ZTDs can be decreased by about 8.1% compared to the GPS-only solution. In the combined GPS/GLONASS/Galileo/BDS

solution for different IGS-RT services, the shortest initialization time of around 480 s has been achieved for the retrieved RT ZTD estimates in the case of GFZC2. The averaged accuracy of the RT ZTD estimates for all available stations can be improved to about 5.06 mm in the multi-GNSS solution with fixing station coordinates. Owing to the addition of multi-GNSS observables, the improvement in the accuracy of the real-time estimated ZTDs can reach about 22.2% compared to the GPS-only solution. For the multi-GNSS real-time retrieving tropospheric delays, the ZTD accuracy in the fixing coordinate mode can be improved by a factor of approximately 2.7 in comparison to that in the kinematic mode.

Acknowledgments: Thanks go to the International GNSS service (IGS) for providing multi-GNSS RT data and product streams.

Author Contributions: Cuixian Lu and Galina Dick conceived and designed the experiments; Gen Liu and Xinyuan Jiang performed the experiments; Cuixian Lu and Gen Liu analyzed the data; Cuixian Lu and Gen Liu wrote the paper; Kai Zheng, Xinghan Chen, Jens Wickert and Harald Schuh helped modify the paper.

Conflicts of Interest: The authors declare no conflict of interest.

References

1. Niell, A.E.; Coster, A.J.; Solheim, F.S.; Mendes, V.B.; Toor, P.C.; Langley, R.B.; Upham, C.A. Comparison of measurements of atmospheric wet delay by radiosonde, water vapor radiometer, GPS, and VLBI. *J. Atmos. Ocean. Technol.* **2001**, *18*, 830–850. [CrossRef]
2. Teke, K.; Böhm, J.; Nilsson, T.; Schuh, H.; Steigenberger, P.; Dach, R.; Heinkelmann, R.; Willis, P.; Haas, R.; Espada, S.G.; et al. Multi-technique comparison of troposphere zenith delays and gradients during CONT08. *J. Geodesy* **2011**, *85*, 395–413. [CrossRef]
3. Bevis, M.; Businger, S.; Herring, T.A.; Rocken, C.; Anthes, R.A.; Ware, R. GPS meteorology: Remote sensing of atmospheric water vapor using GPS. *J. Geophys. Res.* **1992**, *97*, 15787–15801. [CrossRef]
4. Rocken, C.; Van Hove, T.; Ware, R.H. Near real-time GPS sensing of atmospheric water vapor. *Geophys. Res. Lett.* **1997**, *24*, 3221–3224. [CrossRef]
5. Fang, P.; Bevis, M.; Bock, Y.; Gutman, S.; Wolfe, D. GPS meteorology: Reducing systematic errors in geodetic estimates for zenith delay. *Geophys. Res. Lett.* **1998**, *25*, 3583–3586. [CrossRef]
6. Gendt, G.; Dick, G.; Reigber, C.; Tomassini, M.; Liu, Y.; Ramatschi, M. Near real time GPS water vapor monitoring for numerical weather prediction in Germany. *J. Meteorol. Soc. Jpn.* **2004**, *82*, 361–370. [CrossRef]
7. Li, X.; Dick, G.; Ge, M.; Heise, S.; Wickert, J.; Bender, M. Real-time GPS sensing of atmospheric water vapor: Precise point positioning with orbit, clock and phase delay corrections. *Geophys. Res. Lett.* **2014**, *41*, 3615–3621. [CrossRef]
8. Lu, C.; Li, X.; Nilsson, T.; Ning, T.; Heinkelmann, R.; Ge, M.; Glaser, S.; Schuh, H. Real-time retrieval of precipitable water vapor from GPS and BeiDou observations. *J. Geodesy* **2015**, *89*, 843–856. [CrossRef]
9. Zumberge, J.F.; Heflin, M.B.; Jefferson, D.C.; Watkins, M.M.; Webb, F.H. Precise point positioning for the efficient and robust analysis of GPS data from large networks. *J. Geophys. Res.* **1997**, *102*, 5005–5017. [CrossRef]
10. Li, X.; Ge, M.; Zhang, H.; Wickert, J. A method for improving uncalibrated phase delay estimation and ambiguity-fixing in real-time precise point positioning. *J. Geodesy* **2013**, *87*, 405–416. [CrossRef]
11. Dousa, J.; Vaclavovic, P. Real-time zenith tropospheric delays in support of numerical weather prediction applications. *Adv. Space Res.* **2014**, *53*, 1347–1358. [CrossRef]
12. Yuan, Y.; Zhang, K.; Rohm, W.; Choy, S.; Norman, R.; Wang, C.S. Real-time retrieval of precipitable water vapor from GPS Precise Point Positioning. *J. Geophys. Res. Atmos.* **2014**, *119*, 10044–10057. [CrossRef]
13. Real-Time PPP Demonstration Campaign. Available online: http://www.pecny.cz/COST/RT-TROPO/about.php (accessed on 1 April 2015).
14. Montenbruck, O.; Steigenberger, P.; Khachikyan, R.; Weber, G.; Langley, R.B.; Mervart, L.; Hugentobler, U. IGS-MGEX: Preparing the ground for multi-constellation GNSS science. *Inside GNSS* **2014**, *9*, 42–49.
15. Li, X.; Dick, G.; Lu, C.; Ge, M.; Nilsson, T.; Ning, T.; Wickert, J.; Schuh, H. Multi-GNSS meteorology: Real-time retrieving of atmospheric water vapor from BeiDou, Galileo, GLONASS, and GPS observations. *IEEE Trans. Geosci. Remote Sens.* **2015**, *99*, 1–9. [CrossRef]

16. Ding, W.; Teferle, F.N.; Kazmierski, K.; Laurichesse, D.; Yuan, Y. An evaluation of real-time troposphere estimation based on GNSS Precise Point Positioning. *J. Geophys. Res. Atmos.* **2017**, *122*. [CrossRef]
17. Laurichesse, D. The CNES real-time PPP with un-differenced integer ambiguity resolution demonstrator. In Proceedings of the ION GNSS 2011, Portland, OR, USA, 19–23 September 2011.
18. Kouba, J. A Guide to Using International GNSS Service (IGS) Products. 2009. Available online: http://igscb.jpl.nasa.gov/igscb/resource/pubs/UsingIGSProductsVer21.pdf (accessed on 30 April 2009).
19. Zhang, X.; Li, X.; Guo, F. Satellite clock estimation at 1 Hz for realtime kinematic PPP applications. *GPS Solut.* **2012**, *15*, 315–324. [CrossRef]
20. Dach, R.; Schaer, S.; Hugentobler, U. Combined multi-system GNSS analysis for time and frequency transfer. In Proceedings of the European Frequency Time Forum, Braunschweig, Germany, 27–30 March 2006.
21. David, A. Maximum likelihood approaches to variance component estimation and to related problems. *J. Am. Stat. Assoc.* **1997**, *72*, 320–338.
22. Böhm, J.; Niell, A.; Tregoning, P.; Schuh, H. Global mapping function (GMF): A new empirical mapping function based on numerical weather model data. *Geophys. Res. Lett.* **2006**, *33*, L07304. [CrossRef]
23. Saastamoinen, J. Contributions to the theory of atmospheric refraction—Part II. Refraction corrections in satellite geodesy. *Bull. Géodésique* **1973**, *47*, 13–34. [CrossRef]
24. Li, X.; Zus, F.; Lu, C.; Ning, T.; Dick, G.; Ge, M.; Wickert, J.; Schuh, H. Retrieving high-resolution tropospheric gradients from multiconstellation GNSS observations. *Geophys. Res. Lett.* **2015**, *42*, 4173–4181. [CrossRef]
25. Lagler, K.; Schindelegger, M.; Böhm, J.; Krásná, H.; Nilsson, T. GPT2: Empirical slant delay model for radio space geodetic techniques. *Geophys. Res. Lett.* **2013**, *40*, 1069–1073. [CrossRef] [PubMed]
26. GNSS Data Center. Available online: http://igs.bkg.bund.de/ntrip/download (accessed on 15 March 2008).
27. Elsobeiey, M.; Al-Harbi, S. Performance of real-time precise point positioning using IGS real-time service. *GPS Solut.* **2016**, *20*, 565–571. [CrossRef]
28. IGS MGEX. Available online: http://igs.org/mgex (accessed on 25 October 2012).
29. Zhao, Q.; Guo, J.; Li, M.; Qu, L.; Hu, Z.; Shi, C.; Liu, J. Initial results of precise orbit and clock determination for COMPASS navigation satellite system. *J. Geodesy* **2013**, *5*, 475–486. [CrossRef]
30. Steigenberger, P.; Hugentobler, U.; Loyer, S. Galileo orbit and clock quality of the IGS Multi-GNSS Experiment. *Adv. Space Res.* **2015**, *55*, 269–281. [CrossRef]
31. Montenbruck, O.; Steigenberger, P.; Prange, L.; Deng, Z.; Zhao, Q.; Perosanz, F.; Romero, I.; Noll, C.; Stürze, A.; Weber, G.; et al. The Multi-GNSS Experiment (MGEX) of the International GNSS Service (IGS)—Achievements, prospects and challenges. *Adv. Space Res.* **2017**, *59*, 1671–1697. [CrossRef]
32. Montenbruck, O.; Hauschild, A.; Steigenberger, P.; Hugentobler, U.; Teunissen, P.; Nakamura, S. Initial assessment of the COMPASS/BeiDou-2 regional navigation satellite system. *GPS Solut.* **2012**, *17*, 211–222. [CrossRef]
33. Dach, R.; Hugentobler, U.; Fridez, P.; Meindl, M. *Bernese GPS Software Version 5.0*; Astronomical Institute, University of Bern: Bern, Switzerland, 2007.
34. Offiler, D. *Product Requirements Document Version 1.0—21 December 2010*; EIG EUMETNET GNSS Water Vapour Programme (EGVAP-II); Met Office: Exeter, UK, 2010.